JOURNAL OF MATERIALS SCIENCE 23 (1988) 4217–4230

High-dose ion implantation of ceramics: benefits and limitations for tribology

S. J. BULL†, T. F. PAGE*
Department of Materials Science and Metallurgy, University of Cambridge, Pembroke Street, Cambridge CB2 3QZ, UK

Ion implantation is known to be capable of modifying the surface and near-surface physical, chemical and mechanical properties of solids pertaining to hardness and wear. This paper is concerned with such effects of ion implantation into sapphire and soda–lime–silica glass. It establishes the complex interplay between radiation damage, hardness, surface stress and, for the first time, friction. For sapphire, both the shallow indentation hardness response and the integrated near-surface stress increase with damage and exhibit maxima as the surface eventually amorphizes. For the glass, initial damage is shown to result in structural softening before rehardening at higher doses. The radiation-induced stress in the glass is a complex function of dose and seems partly linked to electronic rather than displacement processes. Some structural change also eventually occurs in the glass akin to amorphization in crystals and is accompanied by changes in hardness and surface stress. Superimposed on these patterns of behaviour are changes in the friction behaviour, part of which is ascribed to increased adhesion presumed due to implantation changing the surface affinity for water adsorption. These effects are demonstrated and discussed in the context of ion-implanted ceramics finding application as controlled friction and/or wear components in engineering applications. A number of caveats are established for such applications. Other effects such as gas bubble formation, crazing and sputtering are shown to lead to surface microstructures which can also play a deleterious role in tribological behaviour.

1. Introduction

The wear behaviour of solids is primarily a function of the mutual responses of the contacting surfaces (e.g. [1, 2]), with particular importance given to mechanical properties, microstructural state and topography, though physical and chemical properties may also be important. As ion implantation is a process whereby all these near-surface and surface characteristics may be controllably altered, it would seem to be an ideal technique for modifying the wear resistance of materials. Indeed ion implantation has been used to decrease both the friction and wear of a range of metals and cemented carbides (e.g. [3–12]) in situations where the rate of surface removal is small compared to the shallow depth (typically $\sim 0.1\ \mu m$) of the implantation-affected layer.

Ion implantation is known to produce compositional microstructural and mechanical changes in the surface and near surface regions of materials (e.g. [13–22]). For ceramics these changes may encompass solid solution formation, the accumulation of radiation damage with progressive structural degradation until eventual amorphization, or even the formation of new phases, particularly if ion implantation is combined with some post-implantation annealing treatment (e.g. [17]). Allied to this, the radiation damage caused by both the implanted ions and the displaced substrate atoms may further radiation-harden the surface. The dilation caused by both this damage and the implanted ions themselves is also known to induce surface compressive stresses which will act to oppose the nucleation and growth of surface cracks. However, while several studies of the change in surface structure and deformation behaviour have been published, comparatively little has been reported regarding the concomittant friction behaviour associated with these changes in deformation response.

The majority of previous work has concentrated on the use of low load microhardness testing to characterize the surface mechanical properties of implanted ceramics (e.g. [13, 14, 16–20]). In this way the hardening due to both radiation damage and solid solution effects has been demonstrated. However, at the onset of amorphization, this hardening is modified by the progressive development of a softer amorphous layer. At higher damage levels, the amorphous layer totally dominates the hardness response and an absolute softening of the surface is observed (compared to the unimplanted material). At higher indentation loads, the characteristic crack arrays formed around Vickers

**Present address*: Department of Metallurgy and Engineering Materials, University of Newcastle-upon-Tyne, Newcastle-upon-Tyne, NE1 7RU, UK. †Materials Development Division, Harwell Laboratory, UKAEA, Didcot, Oxon, OX11, ORA.

0022–2461/88 $03.00 + .12

hardness indentations has been used to follow the changes in fracture behaviour of these hard, brittle materials. Thus the surface compressive stresses have been shown to reduce the amount of radial/median crack propagation and also prevent lateral crack break out [22].

With regard to friction, some earlier work by Burnett and Page [23] has shown an increase in the coefficient of friction between implanted sapphire and metal pins at doses below the amorphization dose. Hartley [24] has investigated the friction of implanted diamond on diamond and reported that the effects of implantation on friction were inconclusive, though there may be some slight reduction in the friction coefficient.

The present programme, of which the study reported here forms part, is extending these various approaches towards a fully integrated understanding of the range of effects of ion implantation on the hardness, friction and wear of ceramic materials. This paper demonstrates and establishes the complex interrelationships between damage structure, surface stress, hardness and, for the first time, friction for ion-implanted single-crystal sapphire and soda-lime-silica glass. It also presents a number of caveats for using ion-implanted ceramics in tribological applications.

2. Experimental procedure

Commercial soda-lime-silica glass microscope slides were cut into 20 mm × 10 mm × 1 mm slices, ultrasonically cleaned and degreased in alcohol. These specimens were then implanted with 300 kV argon and potassium ions in the Cockcroft Walton facility at AERE, Harwell. Wafers of $\{1\,0\,\bar{1}\,2\}$ device substrate-grade sapphire (courtesy GEC Wembley) were cleaved into similar sized pieces and cleaned and degreased in a similar manner before implantation with 300 kV yttrium, zirconium and titanium ions. The sapphire wafers were supplied with one side polished to a mirror finish, and apart from degreasing, no further surface treatments were performed prior to implantation. One of the polished surfaces of the microscope slides was abraded with SiC paper to identify the unimplanted surface. Again, apart from cleaning and degreasing, no other surface treatments were performed before implantation. All implantations were carried out at room temperature with a beam current of a few microamps; the maximum specimen temperature rise due to implantation of even a poor thermally conducting specimen was estimated to be 250° C [25]. Implantation usually produces approximately Gaussian concentration and damage profiles below the surface [26]. For the species–substrate combinations used here, the average range and standard deviation of these profiles is given in Table I; R_p is the mean range of the peak of the concentration profile with range straggling (deviation) ΔR_p, similarly X_d and ΔX_d describe the damage profile. These values have been computed from the EDEP-1 computer code of Manning and Mueller [27].

For the glass substrates, argon and potassium were chosen as implantation species because they are of similar mass numbers (and hence similar damage characteristics) but different behaviour in the substrate (potassium may be incorporated into the structure as a network modifier, argon is inert and was expected to produce gas bubbles). For the sapphire samples, yttrium and zirconium have similar mass numbers (and expected damage distribution) while titanium, zirconium and yttrium were expected to have different oxygen affinities and thus should produce different structures during subsequent heat treatment [28].

TABLE I Concentration and damage profile parameters

Target	Ion	Atomic weight	Energy (keV)	R_p (μm)	ΔR_p (μm)	X_d (μm)	ΔX_d (μm)
Sapphire	Y	88.9	300	0.081	0.023	0.046	0.028
Sapphire	Zr	91.2	300	0.079	0.023	0.045	0.028
Sapphire	Ti	47.9	300	0.143	0.041	0.088	0.051
Glass	Ar	39.9	300	0.256	0.067	0.213	0.077
Glass	K	39.1	300	0.243	0.065	0.202	0.074

Microhardness indentations were performed with a Leitz Miniload 2 microhardness tester. All indentations were made under standard conditions (ambient temperature, humidity 50 to 80%, laboratory air, 15 sec dwell time) and, for the sapphire specimens, the long indentor diagonal (Knoop) or one of the indentor diagonals (Vickers) was aligned with $[0\,1\,\bar{1}\,2]$ in order to remove the effects of hardness anisotropy. To follow the change in surface hardness, low load Knoop indentations were used at loads of 10 and 25 gf for the soda-lime glass and 25 and 50 gf for the sapphire. At these loads the long indentation diagonal is typically $\sim 15\,\mu$m giving a penetration depth of $\sim 0.5\,\mu$m and thus the indentation would be expected to lie predominantly in the implanted layer. For statistical reliability, six indentations were performed at each load. After indentation and prior to measurement all specimens were lightly gold coated to increase the reflectivity of the surface.

For measuring the changes in surface stress state, the changes in the lengths of the radial cracks around 100 to 500 gf Vickers hardness indentations, compared to the unimplanted state, were carefully measured. This can be related to the surface stress state using the approach of Lawn and Fuller [29] via the equation

$$2\psi\sigma_s d^{1/2}/K_c = 1 - (C_0/C)^{1/2} \quad (1)$$

where K_c is the local indentation toughness, ψ is a crack geometry term (ψ can be taken to be unity [29]), σ_s is the surface stress, d is the thickness of the stressed layer and C_0 and C are the lengths of the radial cracks in unimplanted and implanted materials respectively. This is known to underestimate the stresses [30] but should predict the correct trends. Because this is necessarily an average over the implanted layer, the surface stress, σ_s, was converted to an integrated stress by multiplying by the thickness of the stressed layer (assumed to be $\sim 4\Delta X_d$ [28]). For the $(1\,0\,\bar{1}\,2)$ sapphire specimens, Burnett and Page [14] have given a detailed description of the cleavage crack geometries expected. In the present case, only the well-developed $\langle 0\,\bar{2}\,2\,1\rangle$ traces of the $\{\bar{1}\,1\,0\,2\}$ cracks were measured because the other crack system present would probably have a

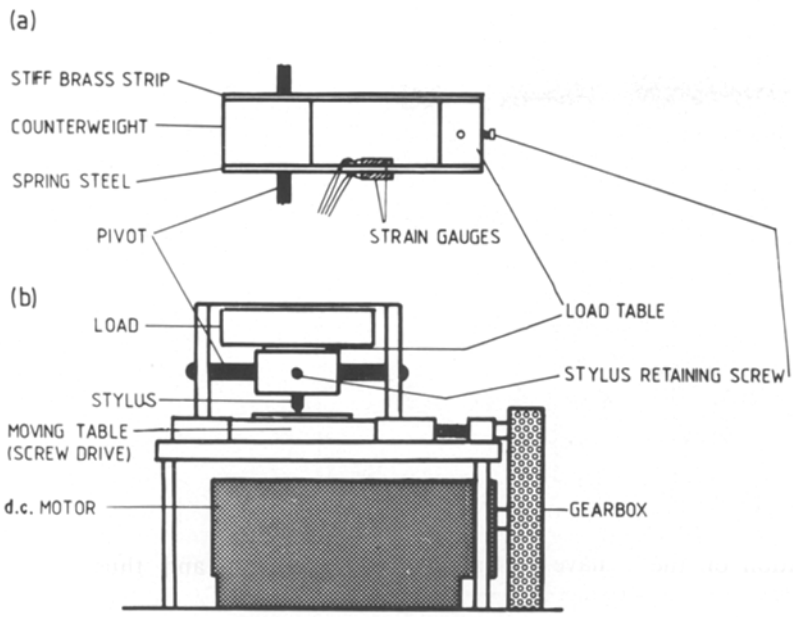

Figure 1 Schematic diagrams of (a) the top view of the stylus retaining arm and (b) the complete scratch rig (i.e. the arm, load and specimen translation assemblies) shown from the front.

different work of fracture. Cracks ending close to the indentation or showing significant branching were ignored. All well-developed cracks were measured for the glass specimens. In all cases sufficient indentations were performed to obtain 20 crack measurements. This involved large numbers of indentations in the implanted glass cases, where cracking only occurred occasionally at the loads used (500 gf) and increasing the load rendered the crack size increasingly large compared to the dimensions of the stressed layer. Measurements were made by reflected light microscopy and a few were subsequently confirmed by SEM. In this way, and for each case, good agreement of crack lengths was found to within half a micrometre.

The argon- and potassium-implanted glass and yttrium-implanted sapphire specimens were scratched in air, under ambient conditions, on a single-pass scratch rig (Fig. 1, [31]) at a sliding speed of $0.25\,\text{mm}\,\text{sec}^{-1}$. Scratches were made with 90° diamond cones (supplied by Shaw Abrasives). In the as-received state the tips of these cones were found to contain a number of angular asperities that were both smoothed and broken off in the first few scratches made. Thus the cones were "worn-in" by repeated scratching of unimplanted material until no further deformation of the diamond could be detected in the SEM. After this treatment, the ends of all cones were found to be approximately parabolic in cross section. The radius of curvature at the tip was measured to be $\sim 40\,\mu\text{m}$ for the cone used to scratch sapphire and $226\,\mu\text{m}$ for the cone used to scratch glass. The differences are probably due to the differences in manufacture of the cones.

The diamond cone was mounted on the end of a balanced parallelogram arm and pressed on to the surface by a dead-weight load. The tangential forces were measured with a strain gauge assembly on the moving arm of the scratch rig. The specimen was moved linearly beneath the diamond by means of an electrically driven micrometer screw. One element of the balanced parallelogram was made from spring steel, the other of brass to give some rigidity to the arm. The strain gauges were mounted on opposite sides of the spring steel arm, bonded with a proprietary strain gauge cement (Kyowa CC-15A) and connected to an amplifier in a half-bridge configuration. The output was recorded on a chart recorder. The arm was calibrated by dead loading and the response was found to be linear in the range of loads used in the experiment.

Scratches were made up to 8 mm in length, depending on specimen geometry. In the sapphire specimens the scratches were always made in the $[0\,1\,\bar{1}\,2]$ direction in order to avoid errors due to anisotropy. From the chart recorder trace, the tangential force was averaged over the length of the scratch track and divided by the load to produce the coefficient of sliding friction. Loads of 25 and 50 g were used as these were expected to give scratches lying predominantly in the implanted layer.

3. Results and discussion

3.1. Hardness and wear

Fig. 2 shows the variation of Knoop microhardness with dose for the specimens implanted in this study. All show the behaviour which has been noted by ourselves and a number of other workers. [13, 14, 17–20] in that, generally, three regions are of importance. At low doses (at least for the sapphire), the hardness increases due to the increase in radiation hardening (plus some limited solid solution hardening [32]). The hardness continues to increase to a maximum at the onset of amorphization due to the build up of damage in the surface layer. The hardness of the amorphous material has been estimated to be $\sim 60\%$ of that of the bulk [20] and thus, after amorphization the hardness falls as the amorphous layer thickens. At the highest doses there is an absolute softening.

For yttrium-implanted $\{1\,0\,\bar{1}\,2\}$ sapphire, amorphization is known to take place at $\sim 3 \times 10^{16}\,\text{ions}\,\text{cm}^{-2}$ [14, 33]. (The amorphization threshold for sapphire has been found to be markedly dependent on crystallographic orientation and is approximately an order of magnitude lower for (0 0 0 1) surfaces [33, 34].) The

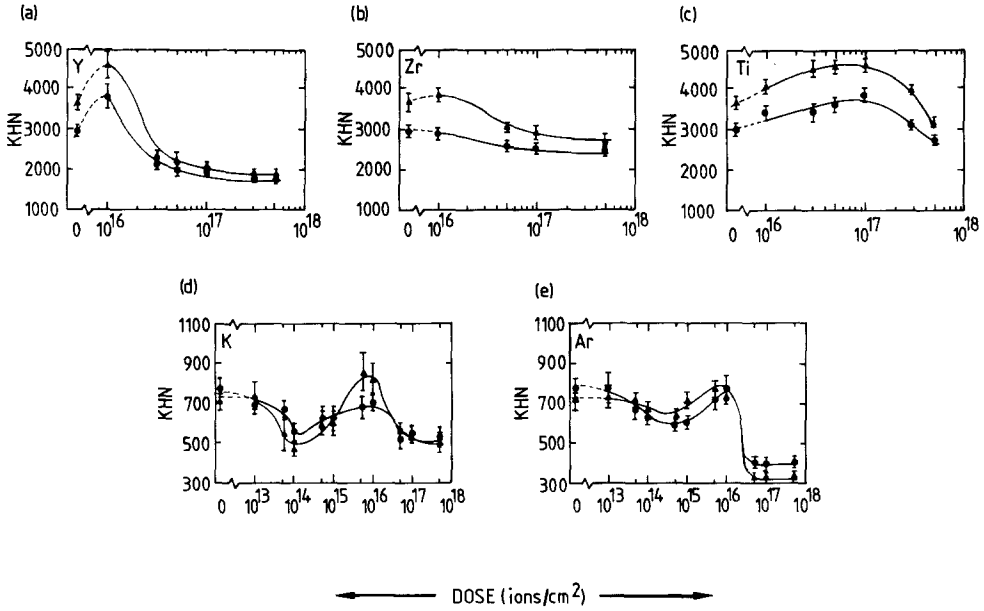

Figure 2 The variation of Knoop microhardness with dose for (a) yttrium-implanted $\{1\,0\,\bar{1}\,2\}$ sapphire (b) zirconium-implanted $\{1\,0\,\bar{1}\,2\}$ sapphire (c) titanium-implanted $\{1\,0\,\bar{1}\,2\}$ sapphire (d) potassium-implanted soda–lime glass and (e) argon-implanted soda–lime glass. The crystalline materials show a single hardness peak before the onset of amorphization whereas the glass specimens show a decrease in hardness at low dose, before developing a similar hardness peak. All implantations were nominally at room temperature (see text). (a)–(c) (▲) 25 g, (●) 50 g; (d), (e) (▲) 10 g, (●) 25 g.

formation of the amorphous layer can be seen in transmission electron microscopy (TEM) samples (Fig. 3) or by Rutherford backscattering (RBS [14]). For crystalline materials, the onset of amorphization is accompanied by a drop in hardness, creating the hardness maxima seen for sapphire in Fig. 2. However, both the argon and potassium-implanted glasses also show a hardness peak followed by a marked reduction in hardness and this seems to suggest some damage-induced structural change occurring, similar to amorphization in crystalline materials. This "amorphization" of the glass specimen is more difficult to understand because the material started in an amorphous state. However, the accumulation of both implanted atoms, and also damage, in the implanted layer will result in a differently-structured amorphous layer with substantially different properties to that of the unimplanted glass. The transition will probably involve significant structural rearrangement and possibly incorporation of the implanted ions into the glass network.

Figure 3 An electron diffraction pattern (TEM, 100 kV) from the near-surface region of $\{1\,0\,\bar{1}\,2\}$ sapphire implanted with 5×10^{17} Y ions/cm^2. The pattern shows diffuse rings characteristic of an amorphous material.

For argon implanted glass, the amorphization phenomenon is accompanied by a very rapid drop in surface hardness which is very different to the behaviour observed for the other implanted materials. However, this rapid softening is due to the formation of a layer of argon bubbles below the surface. These bubbles can be observed at doses above 5×10^{16} Ar ions/cm^2 and are best seen on the surface exposed by exfoliation around hardness indentations (Fig. 4a) or in TEM specimens prepared from the exfoliated debris (Fig. 4b). The size of these bubbles increases with dose. Energy dispersive X-ray microanalysis (EDX) in the scanning electron microscope (SEM) reveals that there is very little detectable argon left in the surface layer once the bubbles have formed. Table II shows the mean bubble radius, r, and the mean bubble separation for all doses where the bubbles could be seen by light microscopy or in the SEM. The pressure, P, of gas in the bubble may be calculated from its radius via

$$P = 2\gamma/r \qquad (2)$$

TABLE II Bubble parameters in argon-implanted glass.

Dose (ions/cm^2)	Mean radius r (μm)	Mean separation (μm)	Mean pressure (MPa)*
5×10^{16}	0.3	0.7	3.3
1×10^{17}	0.5	1.0	2.0
5×10^{17}	1.0	1.3	1.0

*This pressure was calculated assuming a spherical bubble shape. However, it may be that the bubbles are oblate in which case the pressures would be higher (see text).

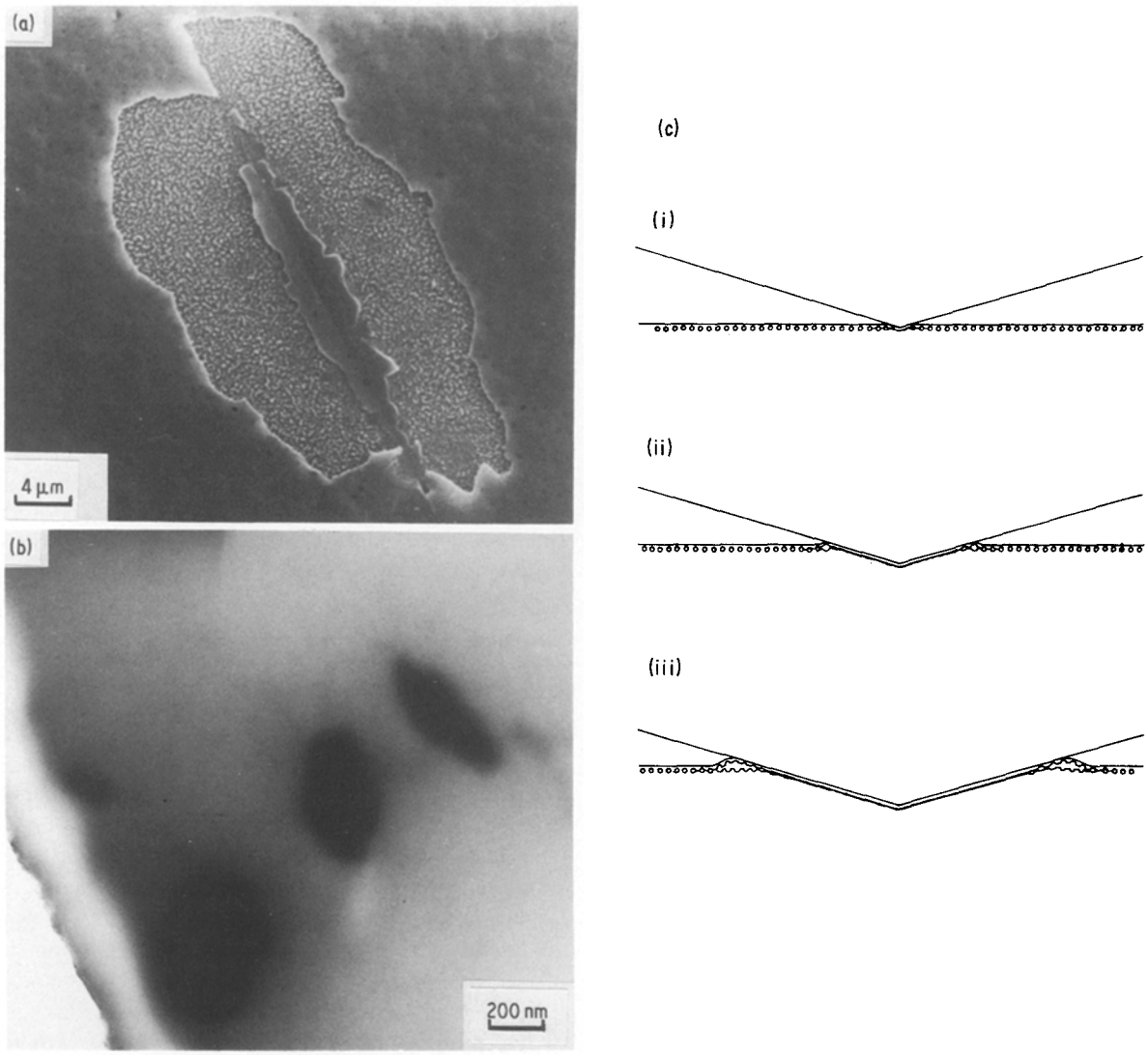

Figure 4 (a) A secondary electron SEM image of a 25 g Knoop microhardness indentation in 5×10^{16} cm^2 implanted glass. A region of material around the indentation has become exfoliated due to the presence of a subsurface argon bubble layer. (b) TEM (100 kV) micrograph of some of the exfoliated material, showing these argon bubbles. The bubbles are darker than the surrounding glass indicating that there is a higher electron density within the bubble than around it. *In situ* EDX analysis reveals predominantly argon in these areas. (c) Schematic diagram of the generation of exfoliated material: (i) bubbles are compressed and connected by fracture parallel to the surface, (ii) the bubbles are compressed flat forcing argon to the edge of the contact area, (iii) the accumulation of argon at the edge of the contact area causes lifting and bending of the material around the indentation, which may fracture and become removed to form the exfoliated material. Because the surface layer is no longer completely attached to the substrate in the indented area, this may be removed on unloading by adhesion to the indentor.

where γ is the surface energy of the bubble. It is likely that this surface energy will be altered by implantation, but as argon is almost insoluble in glass the change is likely to be small. Thus the bubble pressure may be estimated using the surface energy of unimplanted soda-lime glass ($\gamma = 0.5\,\mathrm{J\,m^{-2}}$ [35]). At the lowest doses where bubble formation has just occurred, the bubble layer is nearly continuous, because the bubble separation is nearly the same as the bubble diameter. On loading an indentor on to the surface of an implanted specimen, the bubbles are put into compression (Fig. 4c). The gas pressure inside even the smallest bubbles (3.3 MPa) will be small compared to the indentation pressure of ~ 7 GPa (typical hardness of glass). However, the gas pressure is expected to rise as the bubbles are compressed (assuming the argon does not redissolve) and flattened to a disc-like geometry with sharp edges. This is expected to provide a driving force for the sideways linkage of bubbles to take the configuration of a crack parallel to the surface. The gas is forced out to the edge of the contact area, thus detaching the surface layer from the bulk. The indentation is surrounded by a halo of removed material. This exfoliation of the surface material renders the indentation diagonals impossible to measure accurately (the tendency is to overestimate) resulting in substantially lower hardnesses than might be expected if only "amorphization" were taking place.

For higher doses (e.g. 1×10^{17} Ar ions/cm^2), the bubbles are larger and occupy a larger volume fraction due to the increased amount of argon and the lower bubble pressure [36]. They are expected to be easily compressed. Also the interbubble separation is larger and the compressing of a single bubble will have little effect on the surrounding bubbles. In this case, the implanted layer's deformation properties will be more similar to a spongy porous material. The reduced energy expended in compacting the bubbles leaves

more available for the formation of the indentation and thus the material appears much softer. At the very highest doses (5×10^{17} Ar ions/cm^2), the bubble layer extends to the surface and blistering is observed (see Section 3.4). The sizes of the bubbles seen here are of the same order as the widths of the damage and concentration peaks (taken as $4\Delta X_d$ or $4\Delta R_P$, respectively). However, it may be that the bubbles are confined to the highest damage regions of the material and thus have a flatter shape than assumed. This would result in the internal pressures being considerably higher than shown in Table II.

Hardness has often been promoted as a measure of wear resistance, though there are a number of problems with this (e.g. [37, 38]). For instance Oliver *et al.* [38] have noted that other parameters such as the ductility and toughness of the surface, may be more important in controlling the wear mechanisms of implanted materials. However, in a mild abrasive wear regime where asperities penetrate only a fraction of a micrometre into the surface of a material, the hardness of the surface would be expected to play a large part in the resistance of that surface to wear by plastic ploughing. Thus the increase in hardness at low doses might be expected to increase the wear resistance of the material if plasticity rather than adhesion effects are dominant. At higher doses – where there is some softening due to amorphization – this effect will be negated. Thus, on this criterion alone, it appears that high dose implantation of ceramics would not be a useful treatment for wear resistance.

Further complications arise with the implanted glass because the hardness drops at low doses as can be seen in Figs 2d and e. Mazzoldi [39] has reported that implantation of soda-lime glass with heavy ions results in the depletion of network modifying sodium in the implanted layer. The charged implanted ions appear to free the sodium which diffuses out of the implanted region, this reducing the network strength of the glass in the implanted surface layer. The exact mechanism by which the sodium ions are released is uncertain, though models have been proposed for argon implantation (e.g. [40]). Whereas, in unimplanted modified glasses, deformation would be expected to follow planes with a high density of network modifiers, in the implanted glasses the removal of the modifying ions would be expected to make such deformation easier and thus lower the microhardness of the material. However, our attempt to replace the displaced sodium with the potassium implant still resulted in a similar softening of the material to that occurring with the argon implant, demonstrating the importance of structural disruption in softening. At intermediate doses the effects of radiation hardening begin to dominate and the hardness increases again forming the hardness peak prior to the "amorphization" softening described earlier. However, this radiation-hardened material is only ever as hard as the original unimplanted samples. Thus it would appear that implanting soda-lime glasses can only reduce their wear resistance in terms of both hardness behaviour and the possible deleterious effect of bubble formation with gaseous implant species. However, as will be shown in the next section, the surface toughness of the glass can either be improved or reduced depending on implant dose and species.

3.2. Surface stresses

Fig. 5a shows the integrated surface stresses for the yttrium-implanted sapphire. The compressive surface stress can be seen to increase until amorphization occurs, when there is some stress relief. Indeed at the highest doses the stress levels off and is approximately constant. Microscopy of the high dose specimens reveals that the surface is heavily crazed (i.e. cracked, see Fig. 10) and is almost certainly stress free as was previously reported for yttrium-implanted sapphire by Burnett and Page [14]. Thus what we are, in fact, measuring is the residual stress in the subsurface, uncrazed layer below the amorphous layer. The crazing phenomenon is discussed in more detail in Section 3.4.

The surface stress variation for glass is more complicated (Figs 5b, c) in that both argon and potassium implants produce a stress variation showing two distinct peaks. For the argon case both peaks are compressive, while for the potassium case the first peak is compressive whilst the second is tensile. This is a distinct contrast to the single peak corresponding to amorphization of crystalline ceramics as reported here for sapphire and in previous papers [19, 30]. For both the glass implants, the second peak corresponds to the dose reported for "amorphization" in Section 3.1, while the first peak is at a considerably lower dose.

As the first stress peak occurs at the same dose as the hardness minimum associated with sodium migration induced by electronic radiation damage, it is tempting to postulate that the stress peak has a similar origin. In order to investigate this, the integrated stress was plotted against the energy deposited in both electronic and nuclear processes for our 300 kV argon-implanted glass specimens. Also included are integrated stress data calculated using Equation 1 from the crack lengths (for 500 g loads) measured by Battaglin *et al.* [41] for 50 and 100 kV argon implantation.

The nuclear damage energy density can be estimated by

$$E_{ND} = E_n \phi / (4\Delta X_d) \quad (3)$$

Where E_n is the energy deposited in nuclear damage processes per implanted ion (calculated by the method of Norgett *et al.* [42]), ϕ is the implanted dose and ΔX_d is the damage deviation. This assumes that all of the nuclear damage deposition occurs within $\pm 2\Delta X_d$ of the damage peak (see Fig. 6). Similarly, the electronic damage energy is given by

$$E_{ED} = E_e \phi / X_d \quad (4)$$

where E_e is the energy deposited in electronic processes (i.e. the difference $(E_0 - E_n)$ where E_0 is the ion accelerating energy and E_n is the energy deposited in nuclear damage processes as before) and X_d is the damage range (see Fig. 6). Because the electronic stopping cross-section is greater at high ion energies, it seems reasonable to assume that all the energy lost in electronic processes is lost before the nuclear damage is at a maximum.

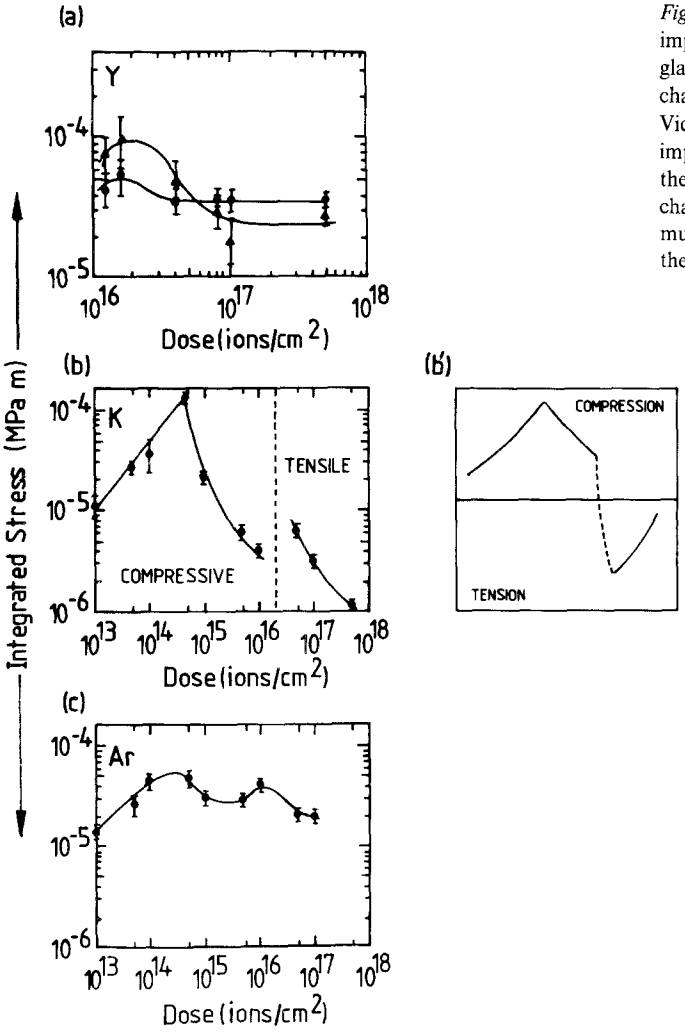

Figure 5 Plots of integrated stress against dose for (a) yttrium-implanted $\{10\bar{1}2\}$ sapphire, (b) potassium-implanted soda–lime glass and (c) argon-implanted soda–lime glass as determined by the change in length of radial cracks around (▲) 100 and (●) 500 g Vickers hardness indentations. The single peak produced by the implantation of crystalline materials is replaced by two peaks for the implanted glasses. In (b), the second peak is complicated by the change in sign of the stress resulting in there being a tensile maximum around a dose of 3×10^{16} K ions/cm^2 with the tensile stress then decreasing at higher doses. This is shown schematically in (b').

In Fig. 7a, integrated stress is plotted against nuclear damage energy density. Here it can be seen that there is a reasonable correspondence between the energy densities of the high dose stress peaks at around 4×10^{22} keV cm^{-3} whereas the correspondence between the positions of the first stress peaks is not so good. Thus this second stress peak is due to the damage caused by displacement processes which is the origin of the single stress peak in crystalline materials.

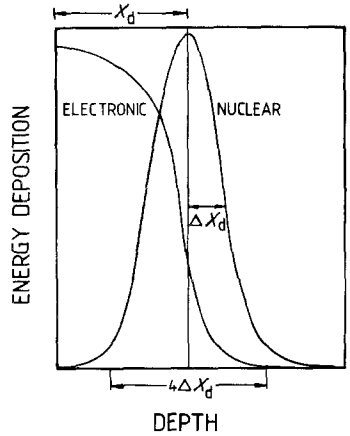

Figure 6 A schematic representation of the energy deposition with depth in materials implanted at medium energies (~ 100 keV). The majority of the electronic damage occurs closer to the surface than the nuclear/displacement damage. X_d is the damage range and ΔX_d its deviation (see Section 2). For the purpose of calculation, it is assumed that virtually all the nuclear (i.e. displacement) damage lies within $\pm 2\Delta X_d$ of the damage maximum (see Equation 3).

For comparison, Fig. 7b shows a plot of integrated stress against electronic damage energy. Here the first stress peaks now show reasonable correspondence at an energy density of 3×10^{21} keV cm^{-3}. Thus the initial stress peak seems to be due to the damage caused by electronic processes, i.e. the processes responsible for freeing the network-modifying sodium and reducing the hardness of the implanted layer as seen in the previous section. The first stress maximum is thus produced at doses where displacement damage begins to be significant and allows structural relaxation of the stress progressively being built up by electronic damage. As the dose is further increased, the volume expansion accompanying increasing displacement damage leads to a second increase in stress, relaxation of which by the "amorphization" process appears to create the second peak.

A further complication is that in the potassium case, this second peak is tensile rather than compressive as might be expected by analogy with crystalline materials. However, tensile stresses generated by the implantation of anomalous glasses have been reported by Eernisse [43]. In such materials, the generation of stress has been attributed to the radiation-induced compaction of the heavily modified glass outweighing the volume expansion effects of radiation-induced defects and implant species accommodation. However, whether this is by bombardment or structural relaxation is unknown.

For wear resistance, the compressive surface stress

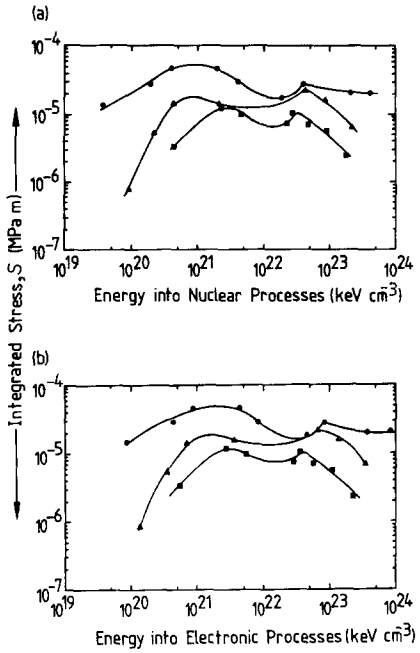

Figure 7 Plots of the variation of integrated stress with (a) energy deposited in nuclear processes (b) energy deposited in electronic processes for soda–lime glass, implanted with argon over a range of energies. Of the two stress peaks, the coincidence of the lower dose peaks is better on the electronic damage plot while the higher dose peaks coincide better when plotted against nuclear damage. The error bars have been removed for clarity but are typified by those in Fig. 5c which shows the same 300 kV results.

is very advantageous because it acts to reduce surface fracture. Fig. 8 shows scratch tracks in unimplanted and 5×10^{17} Y ions/cm^2 implanted sapphire together with surface profilometer traces across these scratches. Although the implanted specimen has a slightly wider scratch track due to the softer surface layer, the amount of radial and lateral cracking around the scratch has been reduced. One of the major mechanisms for material removal in the unimplanted sapphire is the break-out of lateral cracks from the scratch track. Even if these cracks do not reach the surface, they tend to cause upward surface displacements of several micrometres. Subsequently, such projections may be removed if another particle travels across the same area. In fact, lightly brushing the surface of scratched sapphire with a lens tissue can remove a goodly number of such protrusions. The implantation-induced stress field pushes these lateral cracks deeper [14, 22] and thus there is little uplift of the surface.

3.3. Friction and wear

Fig. 9 shows the dose variation of the coefficient of sliding friction, μ. For low-dose yttrium implanted sapphire, the coefficient of friction increases until it is reduced near to the onset of amorphization. At the very highest doses, the coefficient of friction may begin to increase again.

The frictional behaviour of the implanted glass specimens is somewhat more complicated. For the argon-implanted glass there is an increase in the coefficient of friction, up to a dose of 5×10^{14} argon ions/cm^2 when the friction markedly decreases. Above this dose, there is another shallow friction peak at 1×10^{16} argon ions/cm^2 which corresponds to the peak observed in the microhardness behaviour. The large peak at 5×10^{14} Ar ions/cm^2 has no correspondence to anything significant in either the stress or hardness peaks, lying as it does between the doses at which the stress maxima occur (Fig. 5c), and before the hardness maximum (Fig. 2e). For the potassium-implanted glass there is a peak corresponding to the

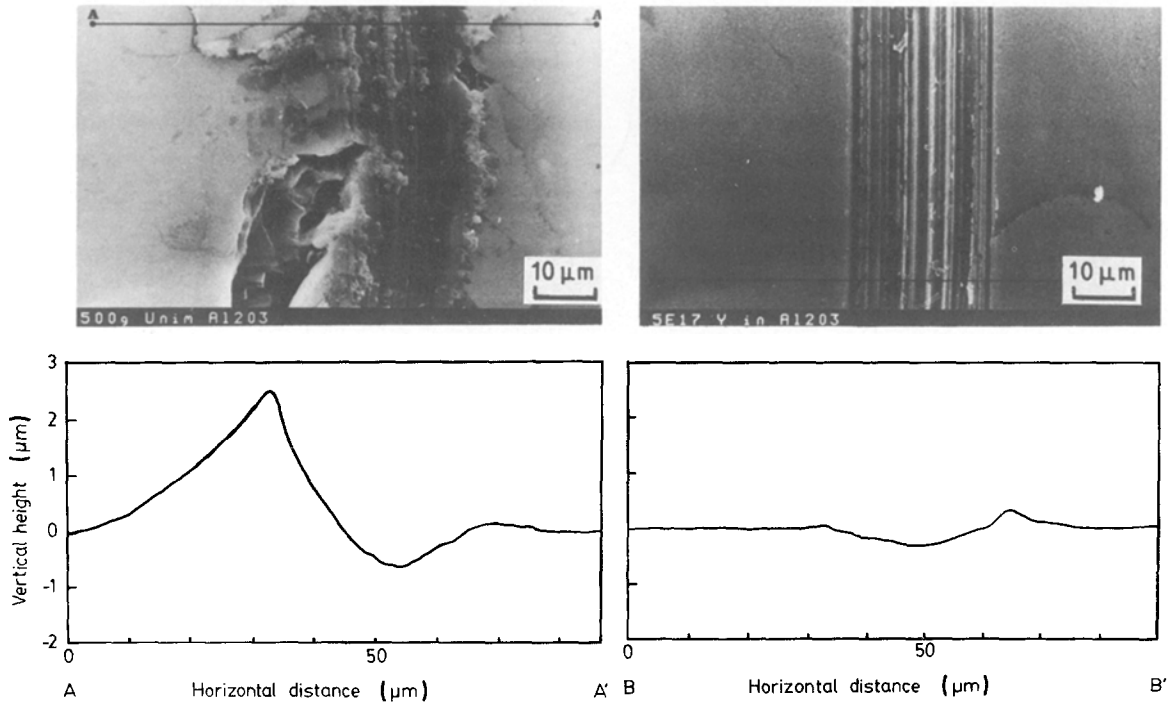

Figure 8 Secondary scanning electron micrographs and surface profilometer traces of 500 g scratches in (a) unimplanted sapphire and (b) 5×10^{17} Y ions/cm^2 implanted sapphire. Subsurface lateral cracking in the unimplanted material causes the surface uplift visible in the profilometer traces. In the implanted specimen, both the radial and lateral cracking around the scratch has been reduced.

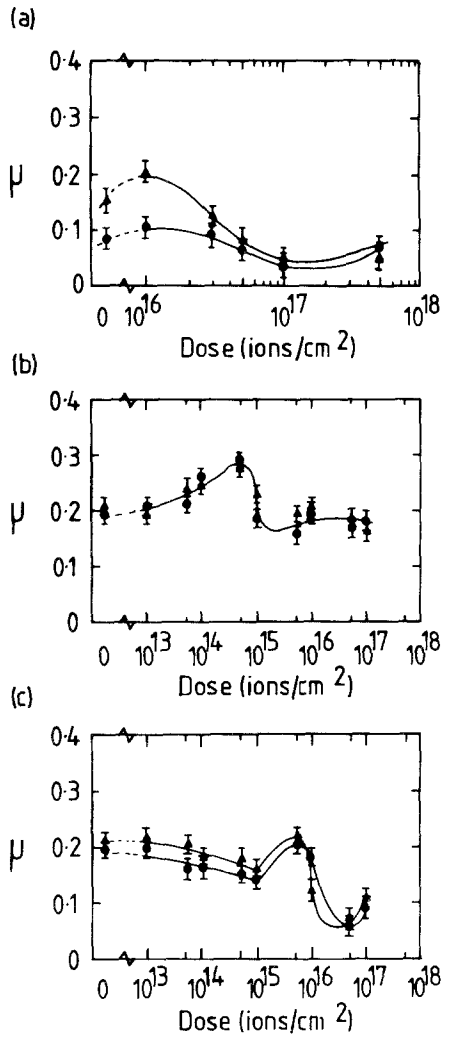

Figure 9 Plots of the coefficient of sliding friction, μ against dose for diamond cones sliding on (a) yttrium-implanted sapphire (b) potassium-implanted soda–lime glass and (c) argon-implanted glass. In the crystalline material there is an increase in friction at low doses, followed by a decrease on amorphization. For the glass implants the behaviour is somewhat more complicated, though there is a similar peak before the onset of "amorphization". (●) 25 g, (▲) 50 g.

hardness maximum at 5×10^{15} K ions/cm^2, but at low doses there is a slight decrease in the coefficient of friction with no peak as in the argon case.

For all specimens further analysis of the friction behaviour in terms of wear track widths demonstrated that another implantation-induced change in behaviour may be controlling at least some aspects of this behaviour. In all cases the widths of the scratch tracks were measured with the microscope system of the microhardness tester. The sapphire specimens show changes in track width as expected from the changes in the microhardness behaviour (i.e. track widths decreasing with increasing hardness). However, the glass specimens show little or no change in track width over all the doses investigated in this study. This is probably due to the larger radius of curvature of the scratching diamond making the scratch difficult to see. However, the scratch is narrow enough that the contribution to the coefficient of friction due to ploughing is likely to be small.

The superficial effects of ploughing are demonstrated in the width of the scratch track produced. For

TABLE III Friction and track width data for yttrium-implanted sapphire (50 gf load)

Dose (ions/cm^2)	μ_{obs}	D (μm)	P' (kg mm^{-2})	Ploughing μ*
0	0.154	8.75	2985	0.089
1×10^{16}	0.203	4.25	3619	0.012
1×10^{17}	0.028	6.75	1930	0.026

*Calculated from Equation 6 assuming plastic ploughing is the dominant wear mechanism.

example, for sapphire at low doses, the track width decreases as expected due to the increase in hardness of the implanted material. Thus, depending on the energy dissipation mechanisms in the softer layer, it might be expected that the contribution to the coefficient of friction due to ploughing would be reduced. However, the coefficient of friction is observed to increase at these doses indicating the dominance of some other mechanism. Bowden and Tabor [1] suggested that the friction properties of materials may be expressed as a combination of the contributions of ploughing through the material and adhesion to it. By their model, the contribution to the friction force produced by ploughing is given by

$$F = D^3P'/12R \quad (5)$$

where D is the track width, R is the radius of the scratching particle, P' is some measure of the yield stress of the material (usually approximated by its hardness) and $F = \mu L$, where L is the load on the scratching particle. For a fixed load and scratch diamond this may be simplified to

$$\mu = kD^3P' \quad (6)$$

where k is a constant. Ion implantation changes both D and P', and so will be expected to change the value of μ. Typical values for D, P' and μ are given in Table III. At low doses D is reduced to around 0.5 of its unimplanted value, whilst P' is increased by a factor of 1.2. Equation 6 predicts that the ploughing component of friction will be decreased to 0.13 times the unimplanted value. However, the measured value of μ has increased by a factor of 1.3. Thus the increase in measured friction at low doses cannot be due to ploughing and hence must be due to increasing adhesion between the scratch diamond and the implanted surface (the topographical changes during low dose implantation have been measured to be minimal). At high doses D is decreased by a factor of 1.2 whilst P' is reduced to around 0.6 of the unimplanted value. This predicts a value for the coefficient of friction much closer to the observed value. Thus friction at high doses seems to be dominated by ploughing through the soft amorphous layer. Further, the decrease in the measured coefficient of friction at the onset of amorphization and the agreement of the coefficient of friction with the ploughing model, implies that the adhesion between the amorphous layer and the scratch diamond is less than that between the diamond and the damaged but crystalline substrate.

These adhesion changes have been confirmed by tests using spheres of a relatively large radius, so that

no scratch track is produced and the contribution due to ploughing is effectively zero [44].

Values of the coefficient of friction for non-metallic materials undergoing dry sliding in air have been found to increase dramatically when the sliding occurs in vacuum [1, 2]. This has been attributed to the removal of various chemical species adsorbed to the surface which have been shown to produce substantial softening in the surface layer [45–47]. Burnett and Page [48] have noted that ion implantation reduces this chemomechanical effect in MgO presumably by altering the affinity of the surface for water in some way, though whether this is due to physical rearrangement of the surface structure, subsurface charge damage or some combination of such effects is still unclear. That the effect is due to something other than the sputtering of adsorbed water from the surface is established by the persistence of the effect long after implantation: samples implanted several years ago still show no chemomechanical effect with water to this day. It thus seems as if the implanted, damaged surface fails to either attract and/or accommodate adsorbed species. It is probable that a similar effect is occuring in both sapphire and glass because both materials are known to form an adsorbed surface-water layer [49, 50]. This layer will have several effects on the frictional behaviour of the material. It may facilitate sliding by physically separating the moving surfaces (hydrodynamic lubrication). This is likely to occur at much smaller loads than used in this study. Alternatively, the monolayer of adsorbate may interfere with the adhesion of the asperities (boundary lubrication). Another important factor is that even very thin adsorbate layers are known to affect the surface plasticity behaviour of alumina and glass to depths of a few micrometres [46, 47]. This depth is comparable to the depth of the scratches produced in this study. However, changes in the coefficient of friction due to ploughing through such a softened surface layer would again be expected to be small compared to the measured changes. It thus seems that ion implantation inhibits the formation of the hydrated layer itself. Although such water-affected layers have low friction, the fact that the softened material is being continually replenished when worn away may lead to unexpectedly high wear rates [37]. Because ion implantation inhibits the formation of such layers, it should reduce this problem but at the expense of higher friction.

A further factor is that metal–ceramic adhesion may be increased when the ceramic contains charged defects such as those produced by ion implantation [51, 52]. If two materials of different dielectric constant are brought together, then the polarization energy of any charge will be affected by the boundary, and an image charge will be induced in the other material. The size of the induced dipole, and hence the adhesion between the two materials, will be a function of the number of such charges, their depth and magnitude and the dielectric constants of the two materials. The damage produced by ion implantation will result in the formation of a number of charged delects in ceramics, and thus it is likely that these defects would give rise to an increased adhesion between the implanted ceramic and a scratching particle of different dielectric constant. This is discussed in more detail elsewhere [44]. Such defects may also be responsible for altering the adsorption behaviour for water. Thus both the effects discussed here (i.e. changes in both chemomechanical effects and charge-driven adhesion) may have their origin in the same damage phenomenon [53]. However, we have been unable to separate these effects further.

These results show that adhesion only increases at low doses because the amorphous material has a poorer adhesion to the scratch diamond than the damaged material and ploughing becomes dominant at high doses. Thus, although ion implantation to low doses may reduce the amount of abrasive wear due to the implantation-induced compressive stresses, the amount of adhesive wear may increase due to the adhesion changes. The change in surface hardness, and hence the change in scratch width, may thus have a relatively small effect on the wear properties of ceramics. Much more important will be the reduction of surface fracture produced by the implantation-induced stresses and the changes in indenter/substrate adhesion. Surface topography may also be important as will be demonstrated in the next section.

In the absence of a better understanding of the structural effects of ion implantation on glasses (e.g. the types of defect involved, the exact consequence of electronic damage and the difference between the various "amorphous" structures apparently occurring) it has been impossible to deduce more concerning the variation of friction between glass and diamond. However, the production of charged defects and the disruption of surface adsorbates might be expected to increase adhesion as observed with the argon-implantation. Why similar effects are not observed with the potassium implant is unknown, and awaits further investigation.

3.4. Surface microstructure

The polished surfaces of all specimens have few visible features and the same may be said for most of the low-dose implants. At the implantation energies used in this study, the gross effects of sputtering on surface topography are negligible. However, for lower energy implants, the microsharpening of existing asperities by sputtering may be important. High-dose implantation, however, tends to produce topographic features by other means and these may affect the wear behaviour.

In yttrium-implanted sapphire, two features are expected to be important, namely crazes and blisters (Fig. 10). The crazes are only found in specimens where an amorphous layer has been formed, and extend from the surface into the damaged but crystalline material below the amorphous layer [14]. However, there is new evidence that these crazes form as a result of thermal expansion mismatch between the sapphire and the amorphous layer rather than by specimen bending as previously reported [14]. If the layer has a larger thermal expansion coefficient than the sapphire (as might be expected for a more open,

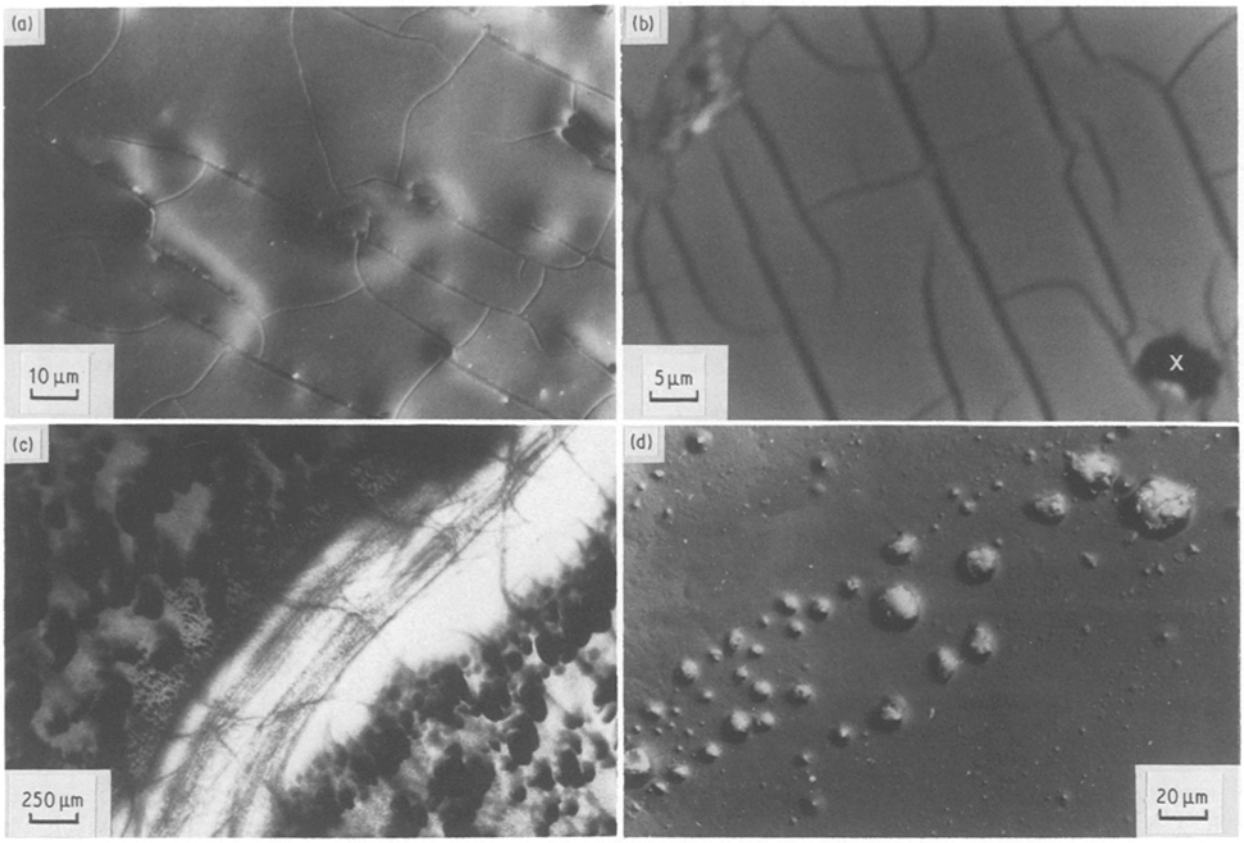

Figure 10 (a) Secondary and (b) backscattered scanning electron micrographs of the crazed regions in 1×10^{17} Y ions/cm^2 implanted sapphire, showing both the craze network and blisters projecting above the specimen surface. The atomic number contrast in the backscattered image indicates that the crazes project through the surface amorphous layer, into the lower atomic number damaged region beneath. Region X marks a blister from which the lid has been removed. (c) a TEM (100 kV) micrograph showing a craze in plan view in 5×10^{17} Y ions/cm^2 implanted sapphire. The material either side of the craze is amorphous, yet the bottom of the craze shows many bend contours and can be shown to be crystalline (by diffraction), if highly stressed [14]. (d) Blisters in 5×10^{16} Y ions/cm^2 implanted sapphire, showing that these form at lower doses where crazing has not occurred.

less well-bonded, damaged structure) and the specimen heats up $\sim 250°$C on implantation, then there will be tensile strains set up in the surface layer of magnitude $\Delta\alpha\Delta T$ on cooling to room temperature. These give rise to the tensile stresses which provide the craze-opening forces in the surface layer. This effect will be discussed in more detail in a further paper [54].

Scratches in the crazed specimens tend to remove material in a different manner to that in uncrazed materials. Fig. 11 shows a 500 g scratch in a 1×10^{17} Y ions/cm^2 implanted sapphire specimen. The scratch track is delineated by the removal of areas of surface material. The measured friction coefficient from this specimen is anomalously high compared to other specimens of similar dose. The material removal is now probably due either to the adhesion of the scratch diamond to a thin damaged but crystalline layer on the subsurface amorphous layer (allowing ready nucleation of cracks in the softer amorphous material and thus aiding surface removal), or to the open edges of the crazes being easily engaged by the scratch diamond thus stressing the amorphous layer in a peeling configuration. For whatever detailed mechanistic reasons, the fact remains that the crazes have promoted gross wear of the surface.

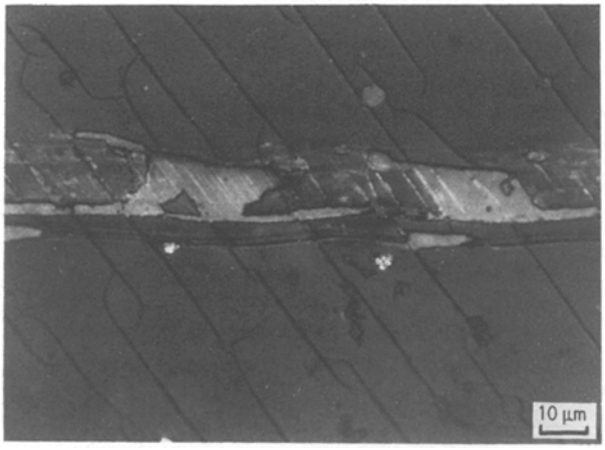

Figure 11 Reflected light micrograph of 500 g scratch in 1×10^{17} Y ions/cm^2 implanted sapphire. The scratch diamond has stripped the amorphous surface layer from the crystalline substrate. The fine striations in the track may either be scratch induced cracks in the substrate, or reveal successive positions of the delaminating crack which removed the surface as the indenter moved over the surface.

As well as the crazes, blisters may be seen in the yttrium-implanted sapphire. Fig. 10 shows these in a 1×10^{17} Y ions/cm^2 implanted specimen but they are also found in all specimens of dose 5×10^{16} Y ions/cm^2 or above. Visible blisters are most common in those specimens where the amorphous layer has reached the surface. Occasionally they may be traversed by a surface profilometer trace and they are measured to be around 0.8 μm high. They are, however, very fragile and a single profilometer trace will rupture the blister leaving a small pit in the surface.

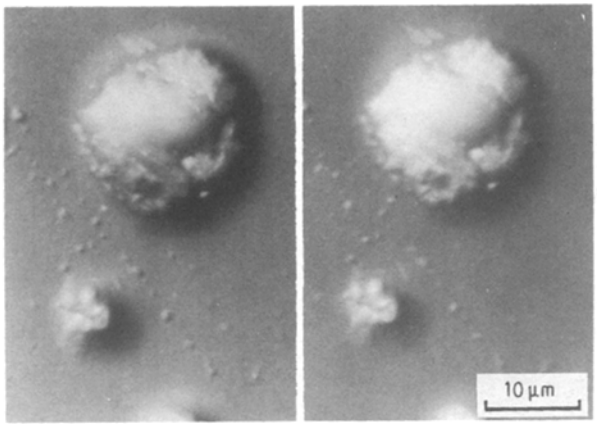

Figure 12 Secondary SEM stereo pair of blisters in 5×10^{17} Y ions/cm^2 implanted sapphire. The blisters are lenticular in cross-section, with some surface cracking, consistent with formation by compressive upward buckling of the substrate.

Fig. 12 shows a stereopair of a blister showing that it is less high than wide in its undisturbed form. This is similar to the blisters observed in high-dose gas implantation of metals [55, 56]. Backscattered SEM images of broken blisters and X-ray microanalysis indicate that the majority of the implanted yttrium lies in the blister cover (e.g. region X in Fig. 10c).

Because the blisters have appeared with a non-gaseous implantation species they must be formed from the damage accompanying implantation, i.e. from the vacancies produced by ion implantation or even gaseous oxygen released from the substrate by the implantation of such a heavy ion at high energy. Auger depth profiles on 5×10^{17} Zr ions/cm^2 implanted sapphire (which has a similar damage concentration to yttrium-implanted sapphire, Fig. 13) show a region where there is a peak in the oxygen concentration. This region of high oxygen density could be responsible for the formation of a blister in this material, though gas may not always be necessary. Early models of blistering (e.g. [57]) were based on forces entirely due to the presence of pressurized gas

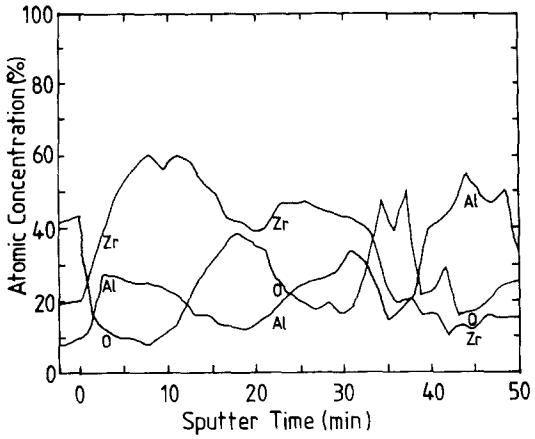

Figure 13 Auger sputter depth profile on 5×10^{17} Zr ions/cm^2 implanted sapphire showing a peak in the oxygen depth profile corresponding to the middle of the implanted zirconium peak (Courtesy Dr I. L. Singer, NRL Washington). The apparent dip in the zirconium profile does not reflect a drop in the number of zirconium atoms but shows the change in concentration as the oxygen level rises.

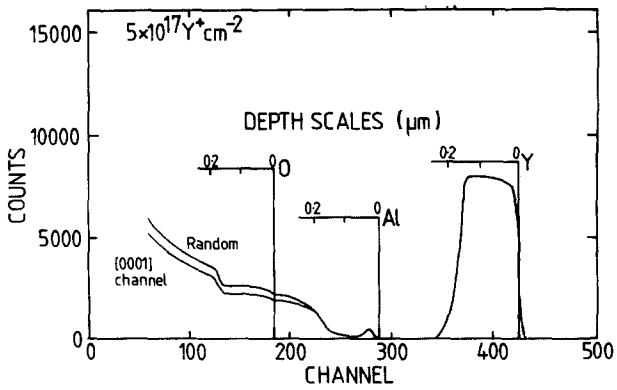

Figure 14 Channelled and aligned RBS profiles of 5×10^{17} Y ions/cm^2 implanted sapphire. There is no evidence for a peak in oxygen concentration below the surface.

in the blister. However, according to Eernisse and Picraux [58], it is lateral compressive stresses that are responsible for blister formation by upwards compressive buckling of the surface layer. As there is no evidence for gas formation in yttrium-implanted sapphire (e.g. from RBS, Fig. 14), this mechanism seems more likely to be occurring in this material.

For yttrium-implanted sapphire the depth of the pit left when a blister bursts can be measured (by surface profilometry) to be about the depth at which the damage profile is a maximum. Nomarski micrographs (e.g. Fig. 15) show that the depth of the pit is comparable to the depth of a craze. Crazes can often be seen running along the edges of blisters, changing their characteristic lenticular shape. Fig. 16 shows a blister in 1×10^{17} Y ions/cm^2. The blister has acted as a nucleation site for crazes which both run out from it radially and skirt the edge of the blister. Because the stresses responsible for formation of the blister during implantation are compressive, it seems unlikely that such cracking should occur. However, the thermal expansion mismatch between the amorphous layer and the substrate which was responsible for the formation of the crazes by creating tensile stresses during post-implantation cooling, should generate sufficient tensile stresses to open crazes around blisters, especially if the blister contains some gas which is keeping it under pressure. Blisters tend to burst when

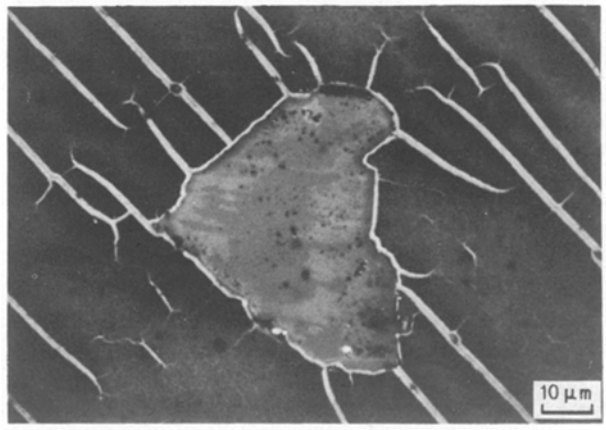

Figure 15 Normarski interference micrograph of a blister from which the lid has been removed in 3×10^{17} Y ions/cm^2 implanted sapphire. One edge of the blister is delineated by a craze, indicating that crazing may alter the shape of a blister.

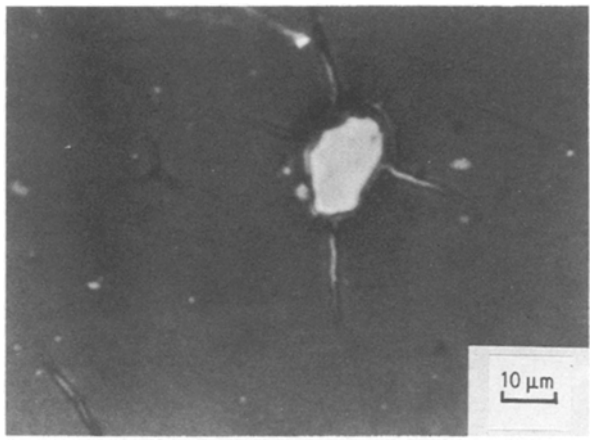

Figure 16 Reflected light micrograph of a blister in 1×10^{17} Y ions/cm^2 implanted sapphire. The blister has acted as a nucleation site for crazes, which both run out radially from it and skirt its edge.

crazing takes place and the detached lid of the blister may lie around on the surface of the material. As both the blister and its debris lie above the surface of the specimen, both are easy sites for the removal of surface material during wear. The raised edges of open blisters would also be expected to contribute to wear in a similar manner to the blisters.

4. Conclusions

Although this is only the first part of a comprehensive appraisal of the factors relevant to the wear of ion implanted ceramics, a number of conclusions may be drawn.

1. For crystalline ceramics, ion implantation leads to both surface hardening (by radiation damage and solid solution formation) together with the generation of compressive surface stresses. The hardness and the stresses go through a single maximum as the surface progressively amorphizes and softens.

2. In modified glasses, implantation leads to a structural softening due to electronic processes allowing sodium-ion migration and network disruption. Increased radiation damage only rehardens the surface to its initial value prior to some surface structural change (akin to amorphization) softening it again at high doses.

3. The surface stress behaviour in glass is a complex function of dose and species. Stress maxima occur at about the "amorphization" dose, but may be either tensile or compressive depending on the implanted ion species. However, a low-dose compressive maximum also occurs which seems to be linked to the same electronic damage process as controls the release of sodium from the glass network and the accompanying hardness peak.

4. The surface hardening produced by ion implantation in crystalline materials at low doses may improve wear resistance in wear regimes where plastic ploughing of the implanted surface by asperities occurs. In implanted soda–lime–silica glasses, the radiation hardening only ever restores the hardness to the unimplanted value after significant softening and thus a similar improvement in wear properties is unlikely.

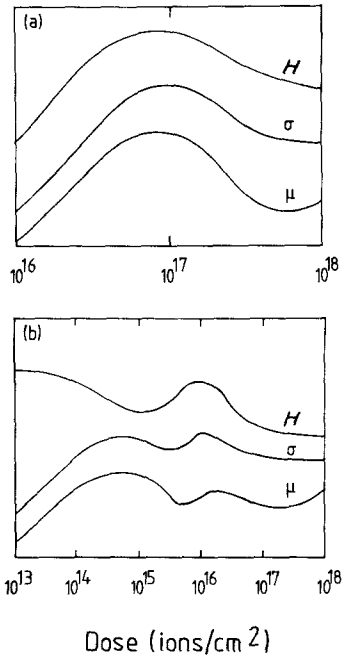

Figure 17 Schematic variation of the hardness H, surface stress σ and coefficient of friction μ with dose for (a) titanium-implanted sapphire and (b) argon-implanted glass. The single peak in these properties at the onset of amorphization in crystalline materials is contrasted with the more complicated behaviour for the glasses.

5. Implantation to low doses increases the adhesion between implanted surfaces and scratching particles due to either the removal of, or disruption of, surface adsorbates and the promotion of surface/slider bonding. The possibility that adhesive wear may now become important will have to be considered if implanted ceramics are to be used in tribological applications.

6. At high contact stresses, where fracture is critical, ion implantation will reduce the wear rate by reducing both asperity fracture, and the cracking around scratches because the compressive stresses generated by ion implantation greatly limit the amount of material removal, both by closing the radial cracks and preventing lateral cracks around scratches from reaching the surface (or, perhaps even nucleating [22]).

7. The effects of sputter-induced micro-sharpening of asperities by ion implantation on the wear of implanted materials is minimal at high implantation energies, but the development of other topographic features such as crazes and blisters can drastically increase the wear rate.

8. Implantation of gaseous ions to high doses can result in the formation of bubble layers in the implanted surface. These layers have poor mechanical properties, promoting a rapid softening of the surface layer and exfoliation of material around indentations.

9. Ion implantation will thus only be useful in wear regimes where the rate of material removal is low enough that the implanted layer is not removed during a components lifetime. This limits ion implantation to use in situations where mild abrasive wear, adhesive wear or chemical wear are important.

10. Because ion implantation can affect abrasive, adhesive, chemical and fracture-dominated wear, it may not simply affect the wear rate for a given mechanism, but lead to changes in the dominant wear

mechanism itself and thus lead to different wear regimes.

In summary, ion implantation can be used to modify surface hardness, surface stresses, surface morphology and friction behaviour. The changes in all these effects are summarized in Fig. 17a for Al_2O_3 and Fig. 17b implanted with the species shown. Quantitative means of estimating the stress and hardness effects have been given for various implant/energy/dose combinations, but the optimum implant will depend critically on the precise balance of properties and behaviour required for a particular tribological application.

Acknowledgements

The authors thank Professor D. Hull F. Eng. for the provision of laboratory facilities at Cambridge and Dr G. Dearnaley for ion implantation at AERE Harwell and for support and helpful critique of this manuscript. Dr I. L. Singer (NRL Washington) is also thanked for the provision of the Auger results. SJB wishes to thank SERC and AERE for the provision of a CASE award.

References

1. F. P. BOWDEN and D. TABOR, "The Friction and Lubrication of Solids", Part 1 (Clarendon, Oxford, 1958).
2. D. H. BUCKLEY and E. RABINOWICZ, Fundamentals of the Wear of Hard Materials, Proceedings of the Conference on Science of Hard Materials 2, Institute of Physics Conference Series No. 75 (The Institute of Physics, Bristol and London, 1986) pp. 825–49.
3. N. E. W. HARTLEY, *Wear* **34** (1975) 427.
4. *Idem, Thin Solid Films* **64** (1979) 177.
5. G. DEARNALEY, *Thin Solid Films* **107** (1983) 315.
6. I. L. SINGER, *Proc. Mater. Res. Soc.* **27** (1984) 585.
7. J. K. HIRVONEN, *J. Vac. Sci. Technol.* **A3** (1985) 2691.
8. P. SIOSHANSI, R. W. OLIVER and F. D. MATTHEWS, *J. Vac. Sci. Technol.* **A3** (1985) 2670.
9. J. T. A. POLLOCK, *Materials Forum* **9** (1986) 127.
10. J. GREGGI and R. KOSSOWSKY, in "A STEM microanalytical investigation of nitrogen implanted cemented WC-Co, Science of Hard Materials", edited by R. K. Viswanadhan, D. J. Rowcliffe and J. Gurland (Elsevier, New York, 1984) pp. 485–97.
11. G. DEARNALEY, *Rad. Eff.* **63** (1982) 1.
12. S. A. DILLICH and I. L. SINGER, *Surf. Coat. Technol.* **29** (1986) 207.
13. P. J. BURNETT and T. F. PAGE, *J. Mater. Sci* **19** (1984) 845.
14. *Idem, ibid,* **19** (1984) 3524.
15. C. J. McHARGUE and C. S. YUST, *J. Amer. Ceram. Soc.* **67** (1984) 117.
16. J. K. COCHRAN, K. O. LEGG and G. R. BALDAU, *Proc. Mater. Res. Soc.* **17** (1983) 549.
17. P. J. BURNETT and T. F. PAGE, *Ibid.* **27** (1984) 401.
18. T. HIOKI, A. ITOH, S. NODA, H. DOI, J. KAWAMOTO and O. KAMIGAITO, *J. Mater. Sci. Lett.* **3** (1984) 1099.
19. T. HIOKI, A. ITOH, M. OKHUBO, S. NODA, H. DOI, J. KAWAMOTO and O. KAMIGAITO, *J. Mater. Sci* **21** (1986) 1321.
20. C. J. McHARGUE, G. C. FARLOW, C. WHITE, J. M. WILLIAMS, B. R. APPLETON and H. NARAMOTO, *Mater. Sci. Engng* **69** (1985) 123.
21. C. J. McHARGUE, *Int. Met. Rev.* **31** (1986) 49.
22. S. G. ROBERTS and T. F. PAGE, *J. Mater. Sci.* **21** (1986) 457.
23. P. J. BURNETT and T. F. PAGE, *Wear* **114** (1987) 85.
24. N. E. W. HARTLEY, *Proc. Mater. Res. Soc.* **7** (1982) 295.
25. P. D. PARRY, *J. Vac. Sci. Technol.* **13** (1976) 622.
26. K. B. WINTERBON, P. SIGMUND and J. B. SANDERS, *Mat. Fys. Medd. Dan. Vid. Selsk.* **37** (14) (1970) 1.
27. I. MANNING and G. P. MUELLER, *Comp. Phys. Commun.* **7** (1974) 85.
28. P. J. BURNETT and T. F. PAGE, Changing the Surface Plasticity and Hardness of Sapphire by Ion implantation, in "Plastic Deformation of Ceramic Materials II", edited by R. E. Tressler and R. C. Bradt (Plenum, New York, 1984) pp. 669–80.
29. B. R. LAWN and E. R. FULLER, *J. Mater. Sci.* **19** (1984) 4061.
30. P. J. BURNETT and T. F. PAGE, *ibid,* **20** (1985) 4624.
31. A. P. MERCER, PhD Thesis, University of Cambridge (1985).
32. A. J. BOURDILLON, S. J. BULL, P. J. BURNETT and T. F. PAGE, *J. Mater. Sci.* **21** (1986) 1547.
33. S. J. BULL, PhD Thesis, University of Cambridge (1987).
34. C. J. McHARGUE, personal communication (1986).
35. A. A. GRIFFITH, *Phil. Trans. Roy. Soc. London* **221A** (1920) 163.
36. P. D. TOWNSEND, J. C. KELLY and N. E. W. HARTLEY, "Ion implantation, sputtering and their applications" (Academic, London, 1976) pp. 84–6.
37. J. T. CZERNUSKA and T. F. PAGE *Proc. Brit. Ceram. Soc.* **34** (1984) 145.
38. W. C. OLIVER, R. HUTCHINGS, J. B. PETHICA, I. L. SINGER and G. K. HUBLER, *Proc. Mater. Res. Soc.* **27** (1984) 603.
39. P. MAZZOLDI, *Nucl. Inst. Meth.* **209/210** (1983) 1089.
40. B. M. SMETTS and T. P. A. LOMMEM, *J. Amer. Ceram. Soc.* **65** (1982) C80.
41. G. BATTAGLIN, R. DAL MASCHIO, G. DELLA MEA, G. DE MARCHI, V. GOTTARDI, M. GUGLIELMI, P. MAZZOLDI and A. PACCAGNELLA, *Nucl. Inst. Meth.* **B1** (1984) 253.
42. M. J. NORGETT, M. T. ROBINSON and I. M. TORRENS, *Nucl. Engng Design* **33** (1975) 50.
43. E. P. EERNISSE, *J. Appl. Phys.* **45** (1974) 167.
44. S. J. BULL and T. F. PAGE, *Nucl. Inst. Meth. in Phys. Rev.* **B32** (1988) 91.
45. N. H. MACMILLAN, Chemisorption-induced changes in the plasticity and fracture of non-metals, in "Surface Effects in Crystal Plasticity", edited by R. M. Latanision and J. T. Fourie (Noordhoff, Leyden, 1977) pp. 629.
46. A. R. C. WESTWOOD, R. D. HUNTINGDON and N. H. MACMILLAN *J. Appl. Phys.* **44** (1973) 5194.
47. A. R. C. WESTWOOD, J. S. AHEARN and J. J. MILLS, *Colloids and Surfaces* **2** (1981) 1.
48. P. J. BURNETT and T. F. PAGE, *J. Mater. Sci. Lett.* **4** (1985) 1364.
49. R. E. HANNEMAN and J. H. WESTBROOK, *Phil. Mag.* **18** (1968) 73.
50. N. H. MACMILLAN and A. R. C. WESTWOOD, Surface Charge-dependent Mechanical Behaviour of Non-metals, in "Surfaces and Interfaces of Glass and Ceramics", edited by V. D. Frechette, W. C. La Course and V. L. Burdick (Plenum, New York, 1974) pp. 493–513.
51. A. M. STONEHAM and P. W. TASKER, *J. Phys. C* **18** (1985) L543.
52. *Idem, Proc. Mater. Res. Soc.* **40** (1985) 291.
53. S. J. BULL and T. F. PAGE, *J. Mater. Sci. Lett.*, in preparation.
54. *Idem,* in preparation.
55. J. ROTH, "Blistering and Bubble Formation", Institute of Physics Conference Series No. 28 (Institute of Physics, Bristol and London, 1976) pp. 280–92.
56. V. M. GUSEV, M. I. GUSEVA, YU. V. MARTYNENKO, A. N. MANSUROVA, V. N. MOROSOV and O. I. CHELNOKOV, *Rad. Eff.* **40** (1979) 37.
57. W. PRIMAK and J. LUTHRA, *J. Appl. Phys.* **37** (1966) 2287.
58. E. P. EERNISSE and S. T. PICRAUX, *ibid.* **48** (1977) 9.

Received 7 December 1987
and accepted 11 March 1988